

AD-R139 687

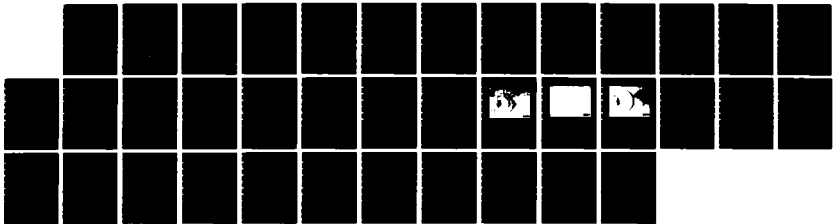
BLAST-WAVE ANALYSIS OF HIGH-PRESSURE COUPLING SHELLS
(U) NAVAL RESEARCH LAB WASHINGTON DC B H RIPIN ET AL.
06 MAR 84 NRL-MR-5279

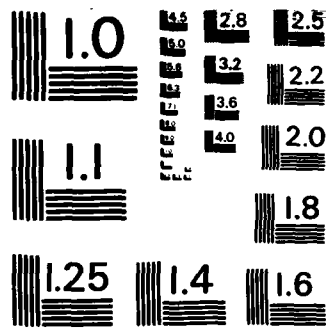
1/1

UNCLASSIFIED

F/G 20/9

NL





MICROCOPY RESOLUTION TEST CHART
NATIONAL BUREAU OF STANDARDS-1963-A

Blast-Wave Analysis of High-Pressure Coupling Shells

B. H. RIPIN, J. A. STAMPER AND E. A. MCLEAN

*Laser Plasma Branch
Plasma Physics Division*

March 6, 1984

This work was sponsored by the Defense Nuclear Agency under Subtask I25BMXIO, work unit 00024 and work unit title "Early Time Plasma."



NAVAL RESEARCH LABORATORY
Washington, D.C.

Approved for public release; distribution unlimited.

AD A139687

DTIC FILE COPY

DTIC
APR 4 1984

84 04 04 077

REPORT DOCUMENTATION PAGE			
1a. REPORT SECURITY CLASSIFICATION UNCLASSIFIED		1b. RESTRICTIVE MARKINGS	
2a. SECURITY CLASSIFICATION AUTHORITY		3. DISTRIBUTION/AVAILABILITY OF REPORT	
2b. DECLASSIFICATION/DOWNGRADING SCHEDULE		Approved for public release; distribution unlimited.	
4. PERFORMING ORGANIZATION REPORT NUMBER(S) NRL Memorandum Report 5279		5. MONITORING ORGANIZATION REPORT NUMBER(S)	
6a. NAME OF PERFORMING ORGANIZATION Naval Research Laboratory	6b. OFFICE SYMBOL (If applicable)	7a. NAME OF MONITORING ORGANIZATION	
6c. ADDRESS (City, State and ZIP Code) Washington, DC 20375		7b. ADDRESS (City, State and ZIP Code)	
8a. NAME OF FUNDING/SPONSORING ORGANIZATION Defense Nuclear Agency	8b. OFFICE SYMBOL (If applicable)	9. PROCUREMENT INSTRUMENT IDENTIFICATION NUMBER	
8c. ADDRESS (City, State and ZIP Code) Washington, DC 20305		10. SOURCE OF FUNDING NOS.	
		PROGRAM ELEMENT NO.	PROJECT NO.
		TASK NO.	WORK UNIT NO. 47-1606-0-4
11. TITLE (Include Security Classification) BLAST-WAVE ANALYSIS OF HIGH-PRESSURE COUPLING SHELLS			
12. PERSONAL AUTHOR(S) B.H. Ripin, J.A. Stamper and E.A. McLean			
13a. TYPE OF REPORT Interim	13b. TIME COVERED FROM _____ TO _____	14. DATE OF REPORT (Yr., Mo., Day) March 6, 1984	15. PAGE COUNT 36
16. SUPPLEMENTARY NOTATION This work was sponsored by the Defense Nuclear Agency under Subtask I25BMXIO, work unit 00024 and work unit title "Early Time Plasma."			
17. COSATI CODES		18. SUBJECT TERMS (Continue on reverse if necessary and identify by block number)	
FIELD	GROUP	Blast-wave Laser-plasma	
	SUB. GR.	Shocks <i>This document</i>	
19. ABSTRACT (Continue on reverse if necessary and identify by block number) The interaction between an energetic laser-produced plasma which streams through an ambient plasma exhibits many properties of a blast wave. We outline the blast-wave theory and find that it compares favorably to many features found in the NRL laser-plasma HANE simulation experiments. Contrary to expectations of an ideal blast wave, however, the laser-produced coupling fronts develop unusual non-uniformities; we speculate on mechanisms that may be responsible for this structure. <i>or speculated</i>			
20. DISTRIBUTION/AVAILABILITY OF ABSTRACT UNCLASSIFIED/UNLIMITED <input checked="" type="checkbox"/> SAME AS RPT. <input type="checkbox"/> DTIC USERS <input type="checkbox"/>		21. ABSTRACT SECURITY CLASSIFICATION UNCLASSIFIED	
22a. NAME OF RESPONSIBLE INDIVIDUAL B. H. Ripin		22b. TELEPHONE NUMBER (Include Area Code) (202) 767-2730	22c. OFFICE SYMBOL Code 4730

CONTENTS

I. INTRODUCTION 1

II. REVIEW OF EXPERIMENTAL FEATURES 2

III. BLAST-WAVE MODEL 4

IV. COMPARISON OF EXPERIMENT WITH BLAST WAVE MODEL ... 11

 Shell Position and Blast-Wave Scaling 11

 Shell Thickness 13

 Shell Density 14

 Shell Temperature 14

V. BLAST-WAVE FRONT NONUNIFORMITIES 15

VI. SUMMARY AND CONCLUSIONS 16

VII. ACKNOWLEDGMENTS 17

 REFERENCES 23



Administrative stamp with fields for "DATE", "BY", "REMARKS", and "SIGNATURE". Includes a handwritten "A-1" and a checkmark.

BLAST-WAVE ANALYSIS OF HIGH-PRESSURE COUPLING SHELLS

I. Introduction

A strong shock can form when an energetic plasma burst expands supersonically into another plasma if the coupling between the two components is strong. The shock propagates through the ambient plasma, sweeping it up into a thin coupling shell which consequently slows down due to the mass accretion. If the initial energy is released quickly compared to the time scales of interest and both particle energy and momentum are conserved, the resulting shock front is termed a Taylor-von-Neumann-Sedov shock⁽¹⁻³⁾ or a "blast wave". Although the self-similar solutions to this problem were motivated by the desire to describe nuclear weapon explosions, the behavior of such coupling shocks and the state of the resulting plasma are also of interest to other disciplines involving sudden releases of large energy. Astrophysics (e.g., supernovae)⁽⁴⁾ and inertial fusion (coupling of pellet explosions to a buffer gas in reactor chambers),⁽⁵⁾ are two such application areas.

In this report we develop features of the blast-wave model and use them to interpret the properties of coupling fronts observed in the NRL laser-plasma experiment.⁽⁶⁻⁸⁾ We find good agreement between experiment and blast-wave theory. However, in contrast to an ideal blast wave, which is often thought to be hydrodynamically stable, the shells in the laser-experiment develop striking spatial structure, often resembling aneurisms, under certain circumstances. The cause of these nonuniformities is not yet isolated; nonetheless, we speculate on some possible responsible mechanisms.

Manuscript approved December 15, 1983.

II. Review of experimental features

In the NRL experiment, laser irradiation of a solid target creates a burst of energetic debris plasma which expands outward into a low-density ambient (stationary) plasma. The initial ambient plasma is created when a background gas surrounding the target is ionized by the radiation (UV and x rays) generated in laser-plasma interaction; subsequent ionization can occur due to radiation emanating from the expanding plasma shell or electron and ion impact. A sketch of the experiment and the distribution functions of the two ion components is shown in Figure 1. Although the experimental arrangement has been described before,⁽⁶⁾ we briefly review the setup.

A (4 ± 1) -nsec pulse from the NRL Pharos II Nd-laser is focused onto a thin (4.6- μm) Al-foil target. The ambient gas used in this series of experiments was usually a mixture of 90% nitrogen and 10% hydrogen gas, but occasionally we used helium instead. A list of the parameters used in these experiments is shown in Table I. Notice that the parameters were varied over a wide range to adequately test the blast-wave model scaling. Also, in some shots a 630 G magnetic field was applied over the interaction volume (transverse to the laser beam). However, no magnetic field dependence was seen in the results to follow. Dark-field shadowgrams were taken of the shock structure at several times after the laser pulse.⁽⁷⁾ Spectroscopic observations were made on similar shots to determine the state (density and temperature) of the ambient and coupling shell plasmas.⁽⁸⁾ Detailed descriptions of these diagnostics and findings are presented elsewhere. Here we concentrate on relating these results to a blast-wave model.

Table I. Parameters used in laser-plasma experiment.

		<u>Range</u>
<u>Laser Energy:</u>	4 - 165 Joules	40x
<u>Ambient Gas:</u>		
Pressure	0.2 - 10 Torr	50x
Molecular weight	28 (N ₂), 4 (He)	7x
<u>Debris:</u>		
Initial velocity	150 - 700 km/sec	5x
Mass (A ₂)	0.1 - 0.5 μgm	5x
<u>Shock Front:</u>		
Observation times	52, 96, 164 nsec	3x
Radii	0.5 - 2.5 cm	5x

Stamper et al.⁽⁷⁾ showed numerous examples of coupling shells, such as the one shown in Figure 2, taken with a dual-time dark-field shadowgraph diagnostic. These photographs indicate that the shells have the following general features:

- o Thin ($\Delta R/R = 0.03$), approximately spherical shocks are observed propagating into the ambient media at times long after the laser pulse has terminated.
- o The shocks decelerate as they propagate away from the focal region.
- o The velocity of the shocks is a function of the deposited laser energy, ambient gas type and, of course, time; but the motion of the shell is insensitive to the initial debris velocity.

However, shells develop structure, such as shown in Figures 3 and 4, at the higher ambient pressures and the lower laser energies. The unperturbed portions of these shells follow the same blast-wave scaling as totally unperturbed shells, but the spatial perturbations appear to accelerate away from the blast-wave position.

The spectroscopic results from McLean et al.⁽⁸⁾ indicate that the ambient plasma is initially weakly ionized (0.2%) at 1-2 eV, one centimeter from the target surface. But just after the blast front arrives the plasma is 100% ionized with a temperature of about 14 eV; the mass density is found to jump above the ambient level by a factor of 10 to 15 at the shell position.

We shall compare these experimental observations with a blast-wave model in the remainder of this paper.

III. Blast-Wave model

The temporal evolution of a spherical blast-wave position looks similar to Figure 5. After the initial energy release the debris rapidly expands, picking up ambient material along the way. After the shell has accreted sufficient mass for us to ignore the initial debris the shell expands and decelerates with the familiar self-similar blast-wave dependence $R \propto (E/\rho)^{1/5} t^{2/5}$. Finally, when the shell velocity approaches the acoustic speed in the ambient media the disturbance is no longer shock-like and it propagates with the speed of sound. There have been many treatments of blast-waves since the first treatments by Taylor, Von Neumann, and Sedov. Some of these works extend the theory into the initial phase, where the debris mass is important,⁽⁹⁾ others are hydrodynamic calculations,^(10,11) and some treat the stability of shock fronts.⁽⁴⁾ We follow the method of Chernyi as outlined in Zeldovich and Raizer.⁽¹²⁾ This blast-wave approximation has been shown to

yield results within a few percent of exact treatments. The following assumptions are made:

1. The energy release is considered an instantaneous point explosion.
2. Spherical symmetry is assumed for simplicity.
3. The debris velocity and shock speeds are much larger than the undisturbed ambient sound speed.
4. The expansion conserves particle energy and momentum.
5. The ambient gas/plasma is swept up by the debris front into a thin cold shell having a mass large compared to that of the initial debris.
6. The media can be characterized by a constant effective ratio of specific heats γ .
7. The counterpressure due to the ambient plasma is negligible.

The shell front is treated as a strong shock wave and, hence, the Hugoniot jump relations apply between the ambient media (o) and shell(s). The density jump is therefore given by

$$\frac{\rho_s}{\rho_o} = \frac{\gamma+1}{\gamma-1} . \quad (1)$$

The flow velocity behind the shock u_s is related to the shock speed V_s by

$$\frac{u_s}{V_s} = \frac{2}{\gamma+1}, \quad (2)$$

giving the pressure within the shock,

$$P_s = \left(\frac{2}{\gamma+1}\right) \rho_o V_s^2. \quad (3)$$

Now, combining the results of the strong shock jump relations with conservation of mass, energy and momentum we obtain many of the blast-wave properties. Conservation of mass is expressed by,

$$4\pi R^2 \Delta R \rho_s = \frac{4\pi R^3}{3} \rho_o + (m_d) = M. \quad (4)$$

The quantity on the left side of Eqn. (4) is the total shell mass as a function of shell radius R and shell thickness ΔR ; on the right side is the mass of ambient gas within the bubble volume (assumed to be completely swept up) plus the initial debris mass m_d (neglected here). The relative thickness of the shell is found by combining Eqn. (4) with Eqn. (1), i.e.,

$$\frac{\Delta R}{R} = \frac{1}{3} \frac{\gamma-1}{\gamma+1}. \quad (5)$$

Proceeding, conservation of momentum is given by,

$$\frac{d}{dt} (M u_s) = 4\pi R^2 P_b. \quad (6)$$

P_b is the pressure within the bubble volume which pushes outward on the

shell. The shell is assumed to have most of the system mass but some small amount of mass must remain inside the shell boundary (bubble). Finally, conservation of energy sets the energy in the explosion E equal to the sum of the shell kinetic energy plus the thermal energy invested in the system; this is expressed as:

$$E = \frac{1}{2} M u_s^2 + \frac{1}{\gamma-1} \frac{4\pi R^3}{3} P_b + \left(\frac{1}{\gamma-1} 4\pi R^2 \Delta R P_s \right). \quad (7)$$

The first term of E is the shell kinetic energy, the second and third terms are the thermal energies within the bubble and shell respectively. The last term (shell thermal energy) is usually neglected* relative to the second term (bubble thermal energy) since the ratio is of order 10^{-1} . We make the same assumption here, however, note that these two contributions to the thermal energy become more comparable as ΔR increases, as P_b decreases or in the event that the γ of the plasma in the bubble is higher than that of the shell (which could be true since the bubble has a much hotter, lower-density plasma than the shell). This assumption about the apportionment of thermal energy does not change the blast-wave $R-t$ scaling - only the constant of proportionality. We shall return to this point later. Demanding that the energy E be independent of radius throughout the expansion and assuming that $P_b \propto P_s$ gives a bubble pressure about half that of the shell pressure P_s , i.e.,

*Note that Harris⁽¹³⁾ made the opposite assumption, i.e., neglecting the bubble energy relative to the shell's kinetic energy. Therefore his results, and those that follow them,⁽⁹⁾ do not apply here.

$$P_b = \frac{1}{2} P_s. \quad (8)$$

[This is compared to $P_b = 0.41 P_s$ for $\gamma = 1.2$ in the exact case.]

Now, from the above relations the expression for the blast-wave radius with time similarity solution is⁽²⁾

$$R(E, \rho_o, t) = \zeta_o (E/\rho_o)^{1/5} t^{2/5}, \quad (9a)$$

or, in "practical" units,

$$R(\text{cm}) = 0.092 \zeta_o [E(\text{J})/(P(\text{Torr})/\text{MW}/\text{MW}_{\text{N}_2})]^{1/5} t(\text{nsec})^{2/5}, \quad (9b)$$

where ζ_o is a function of γ of order unity.. Within our set of assumptions, ζ_o is given by the relation,

$$\zeta_o = \left(\frac{75}{16\pi} \frac{(\gamma-1)(\gamma+1)^2}{(3\gamma-1)} \right)^{1/5}. \quad (10)$$

For completeness we can extend the treatment in Ref. 12 to include the shell thermal energy in the energy balance [third term of Eqn. (7)]. We also allow for the γ of the plasma within the bubble to differ from the shell/ambient plasma γ by designating the bubble γ by γ_b and that of the remaining plasma by γ ; then Eqn. (10) becomes instead,

$$\zeta_o' = \left(\frac{75}{16\pi} \frac{(\gamma_b-1)(\gamma+1)^2}{4\gamma_b + \gamma - 3} \right)^{1/5}. \quad (10')$$

The ratio $(\zeta_o'/\zeta_o)^5$, the ratio in inferred explosive energy release under the two sets of assumptions can differ by about a factor of two although the

possible error in $R(\tau)$ is only 12%. It is clear that detailed hydrodynamic calculations, keeping track of the local values of γ , are necessary to get a precise description of the expansion. Unless otherwise indicated we use Eqn. (10) in the remainder of this paper.

The ratio of thermal energy to kinetic energy in the blast-wave system is interesting; this ratio, obtained by taking the ratio of the second-term to first-term in Eqn. (7), is given approximately by

$$\frac{W_{TH}}{W_{KE}} = \frac{1}{2} \left(\frac{\gamma+1}{\gamma-1} \right) . \quad (11)$$

[The right hand side of Eqn. (11) becomes $\frac{1}{2} [(\gamma+1)/(\gamma_b-1)] + 1$ under the same set of assumptions as Eqn. (10').] Other relevant blast-wave parameters are the plasma effective γ , temperature in the shell and in the bubble volume. The temperature in the shell can be estimated by using an approximation to the internal energy of air,⁽¹²⁾

$$\epsilon = 8.3 T_s (\text{eV})^{1.5} (\rho_A/\rho_s)^{0.12} \text{ eV/molec}, \quad (12)$$

which is valid for temperature T_s between 1 and 25 eV, and density ρ_s between $10 \rho_A$ (ρ_A = atmospheric density) and $10^{-3} \rho_A$; γ ranges from 1.1 to 1.3 for air in this regime⁽¹²⁾ with $\gamma = 1.24$ a good "effective" value. The internal energy is also given by

$$\epsilon = \frac{1}{\gamma-1} \frac{P}{\rho}, \quad (13a)$$

where P and ρ can be determined through Eqns. (1), (3), (8) or direct measurements. Equating Eqn. (13a) to (12), with appropriate units, gives an

estimate for T_s . In the shock front Eqn. (13a) becomes

$$\epsilon = \frac{2V_s^2}{(\gamma+1)^2} \quad (\text{J/kg}), \quad (13b)$$

or, to obtain the same units as Eqn. (12), multiply by $0.334 \times \text{MW}$ and express the shock speed V_s in units of (10^7 cm/sec) . The resulting expression for temperature in the shell is thereby found to be,

$$T_s (\text{eV}) = 4.0 \times \left[\frac{V_s^2 (\times 10^7 \text{ cm/sec}) * \text{MW}}{(\gamma+1)^2 (\rho_A / \rho_s)^{0.12}} \right]^{2/3} \quad (14)$$

A tabulation of some of these blast-wave parameters is given in Table II for $\gamma = 1.2, 1.4, \text{ and } 5/3$. Figure 6 shows exact blast-wave density and temperature for the case of $\gamma = 1.23$ to illustrate how these parameters vary.⁽¹²⁾ Note that, as assumed, most of the mass is in a very thin shell. Also, the high temperature within the bubble is a consequence of the approximate pressure balance with the shell (but with a much lower density). As we go towards the center of the bubble, the plasma density goes to zero as:

$$\rho \sim R^{3/\gamma-1} t^{-6/5(\gamma-1)}, \text{ and the temperature increases as:}$$

$$T \sim R^{-3/\gamma-1} t^{(6/5)(2-\gamma)/(\gamma-1)}. \quad (12)$$

We now compare the experimental findings with the blast-wave model.

Table II. Variation of blast-wave parameters with effective γ .

Parameter	Relation	$\gamma=1.2$	$\gamma=1.4$	$\gamma=5/3$
$\frac{\rho_s}{\rho_o}$	$\frac{\gamma+1}{\gamma-1}$	11	6	4
$\frac{\Delta R}{R}$	$\frac{1}{3} \frac{\gamma-1}{\gamma+1}$	0.03	0.06	0.08
$\frac{W_{TH}}{W_{KE}}$	$\frac{1}{2} \frac{\gamma+1}{\gamma-1}$	5.5	3	2
P_s	$\frac{2}{\gamma+1} \rho_o v_s^2$	($\sim 10^3$ atmospheres at 7 Torr N_2 , $v_s = 100$ km/sec)		
$\frac{P_b}{P_s}$	$\frac{1}{2}$	0.4	0.35	
ζ_o	Eqn. (10)	0.89	1.01	1.12
ζ_o'	Eqn. (10'), $\gamma_b = \gamma$	0.86	0.97	1.06

IV. Comparison of experiment with blast wave model

The main observables in this experimental series, that we will relate to blast-wave theory, are the shell position R , the thickness of the shell ΔR , and density ρ_s and temperature T_s of the shell plasma. Experimental variables included: the laser energy, the laser focal spot size (and thereby the initial debris velocity), the ambient gas type and pressure, the presence or absence of a 630 G magnetic field, occasional variations in the target angle or structure, and the observation times.

Shell position and blast-wave scaling

A plot of the distance R of the shock fronts from the target surface for all of our experimental shots (with the exception of an "odd-ball" shot 13601), which span the range of parameters tabulated in Table I, is shown in

Figure 7; the variables along the abscissa of Figure 7 are scaled according to Eqn. (9b). Note the good agreement of the entire data set with the blast-wave scaling parameter $[(E/\rho_0)t^2]^{1/5}$, with a single universal constant of proportionality, $\zeta_{oe} = 0.123/0.092 = 1.34$ (from Eqn. 9b). The scaling is insensitive to the initial debris velocity for constant incident laser energy.

Unfortunately, for this series of experiments it is difficult to accurately relate the observed ζ_{oe} to theory ζ_o due to our lack of spherical symmetry. Subsequent experiments will improve the symmetry by using smaller, limited mass, targets and, eventually, double-sided illumination. Nonetheless, we shall make a rough comparison between experimental and theoretical ζ_o 's. We make two corrections to the experimental ζ_{oe} . First, the absorption of laser light is about 80-90% not 100%, in our irradiance regime;⁽¹⁴⁾ also, about 90% of the absorbed energy becomes debris energy. Therefore, the energy E in the blast-wave relation should be multiplied by about 0.8. Second, a much larger correction, but less well defined, is to account for the lack of spherical symmetry of the debris expansion. If we use the fact that about half the plasma debris energy is contained within a half-cone angle of 40° from the normal of the target in vacuum^(14,15) and assume that this debris angular distribution still holds true throughout the expansion (this may not be too bad an assumption since the flow is very supersonic), then the ratio of the solid angles between a complete sphere (4π steradian) and the experiment half-energy content cone is about 10. Thus, we must also multiply E by about $10/2 = 5$ (the factor of 2 comes from only half the energy within the 40° cone). Taking the one-fifth power of these two corrective factors together $[(0.8) \times (5)]^{1/5} = 1.32$ and dividing it into ζ_{oe} (1.34) we obtain an equivalent spherical experimental value for ζ_o of $\zeta_o = 1.0 \pm 0.1$.

Assuming complete coupling of the debris energy then yields $\gamma = 1.4 \pm 0.2$ by setting Eqn. (10) equal to $\zeta_0 = 1.0$. If the coupling were reduced then ζ_0 and γ would tend to increase. But Zeldovich and Raizer⁽¹²⁾ claim that γ for air in our density-temperature regime ranges between 1.14 and 1.3. Additionally, we show below that the shell thickness implies a γ of about 1.2. Further, we have shown previously⁽¹⁶⁾ that no distinct debris energy reaches our time-of-flight detectors at 2 Torr, and that most of the debris peak is lost at 200 mTorr.⁽⁶⁾ We conclude, therefore, that the coupling between debris and ambient plasmas for this high pressure regime (0.2 to 10 Torr) is high, perhaps nearly complete.

We note here that the coupling seems much better than that implied by a naive application of the nuclear-elastic and bound-electron stopping powers as presented in Fig. 4.14 of ref. (17). This stopping power curve seems too weak to account for our good coupling by at least an order of magnitude. Prettie also makes this point.⁽¹⁸⁾ Most likely free-electron and possibly plasma phenomena contributions are important in our case.

Shell thickness

The shell thickness-to-radius ratio $\Delta R/R$ is observed to be about 0.03 ± 0.01 . In fact the bright-dark-bright structure seen in the shock front shadowgrams implies a steep gradient on both the front and back surfaces of the shell, consistent with the blast-wave picture shown in Fig. 6. This implies $\gamma = 1.20 \pm 0.07$ from Eqn. (5), a value consistent with both the determination from $R(t)$ above and the equation-of-state of air.⁽¹²⁾ Actually, the shell thickness is a relatively sensitive independent indicator of the effective γ ; for convenience, we invert Eqn. (5) and solve for γ , i.e.,

$$\gamma = \frac{1+3(\Delta R/R)}{1-3(\Delta R/R)} \quad (15)$$

Shell density

McLean et al.⁽⁸⁾ use results from spectroscopic continuum measurements to infer the density of the plasma within the shock front. Typical shell densities are found to be about 10 to 15 times the ambient N₂ density at 1 and 5 Torr fill pressure. The inferred γ from Eqn. (1), given by the expression,

$$\gamma = \frac{(\rho_s/\rho_o)+1}{(\rho_s/\rho_o)-1} \quad (16)$$

yields $\gamma = 1.14$ to 1.22 for the experimental density values. Thus, the density jump at the shell is also consistent with a blast-wave with $\gamma \sim 1.2$ and the other experimental results.

Shell temperature

Shock front temperatures of order 10 eV were estimated by McLean et al.⁽⁸⁾ from the highest ionization state of nitrogen observed. This is also consistent with the blast-wave model, although, presently, neither the measurement nor the theoretical prediction are expected to be very precise. For the temperature within the shock front [using $\gamma = 1.2$, $\rho_A/\rho_s = 100$, $MW = 28$, and a typical shock speed at $R=1$ cm of $V_s = 1 \times 10^7$ cm/sec in Eqn. (14)] is $T_s \approx 9$ eV. This is also in remarkable agreement with experiment.

The very low density plasma within the shell cavity, or bubble, should be at a much higher temperature than T_s . No measurement of T_b was made in this experimental series. But, as an estimate of what to expect, if we assume that the equation-of-state of this plasma continues to follow Eqn. (12) [not likely since Eqn. (12) is based upon the Saha equilibria and the bubble is

closer to coronal equilibrium], then the bubble temperature will be higher than the shell's by a factor of order $(\rho_s/\rho_b)^{0.6}$. This scaling was obtained by assuming pressure balance throughout the blast-wave system, which sets $\epsilon\rho =$ constant. A more accurate air and debris equation-of-state for the bubble plasma is needed for a better estimate. Measurement of T_b is an experimental challenge due to the low density of the bubble plasma within the high density shell.

V. Blast-wave front nonuniformities

What causes the shock front nonuniformities that are observed to develop in the NRL experiment? Why are the nonuniformities, such as in Figs. 3 and 4, so weird? To answer these questions we will require inventive theory and more experiments to eliminate or confirm mechanisms. Listed below are a few speculations.

It is often stated that expanding ideal blast-waves are hydrodynamically stable, yet this statement has not, to our knowledge, been proven in general.⁽¹⁹⁾ It has been proven for a few special cases but not for the γ 's and uniform ambient media of interest here. If the shock fronts are Rayleigh-Taylor unstable for some reason (inherently, or due to differential radiation from swept up debris and ambient plasma⁽¹⁸⁾) the growth-rates can be very large. For example, taking shell decelerations typical of the experiment ($g \sim 5 \times 10^{14}$ cm/sec²) and typical wavelengths observed ($\lambda \sim 3$ mm) yields sufficiently large growth rates, $\gamma_{RT} = (kg)^{1/2} \sim 10^8$ /sec, to create large nonuniformities within typical expansion timescales.

Another possible mechanism, target jetting, favored by C. Longmire⁽²⁰⁾, could cause aneurism-type protrusions. Bumps in the coupling front occur due to the impact of slower target debris with the decelerated

blast wave. We will test this hypothesis in the next experimental series by using thin foils and limited mass targets which should be completely ablated by the laser pulse, thereby eliminating a source of slower debris material.

Keskinen⁽²¹⁾ has proposed interesting asymmetrizing mechanisms caused by the self-generated magnetic fields⁽²²⁾ that may be present during the initial expansion; these magnetic fields modify the flow patterns of the expanding debris plasma.

We hypothesize that if a local thinning of material at the shock front occurs, then that region will be pushed ahead of the thicker regions, as sketched in Fig. 7. If we further hypothesize that either the mass pickup rate is reduced or mass flows away from the tip of this protrusion then the projection will grow nonlinearly. Similar phenomena may occur due to thermal or composition nonuniformities in the shock front.

Other nonuniformity-inducing mechanisms are, no doubt, possible; an understanding of this phenomena awaits further experimentation. It is noted here that some shock front nonuniformities have been seen previously in other laser experiments.^(23,24)

VI. Summary and Conclusions

We have seen that strong-coupled blast-waves are formed at pressures above 200 mTorr in the NRL laser-experiment. These shells are thin ($\Delta R/R \approx 0.03$) dense ($\rho_s/\rho_o \approx 10$) cool ($T_s \approx 10$ eV) and exhibit many properties associated with energy- and momentum-conserving blast-waves.

However, questions remain. What is the source of the structure that develops on the shell, particularly the aneurism-like protrusions? Why do the bumps seem to multiply at later times and higher pressures? What contributes to the good debris-ambient plasma coupling we seem to have? Are free-bound

collisions sufficient or are plasma instabilities, such as the unmagnetized ion-ion or ion acoustic instabilities, operative in this regime? Can we really distinguish our case from a radiating energy-non-conserving (but momentum-conserving) shell?⁽²⁵⁾ Kilb claims that the radius of such a shell scales like $R \sim (V_d t / \rho)^{1/4}$, where V_d is the initial debris velocity. We will attempt to address these and other issues in future work.

VII. Acknowledgments

This work was supported by the Defense Nuclear Agency. The authors thank Drs. W. Ali, D. Book, H. Griem, and S. Obenschain of NRL and R. Kilb and D. Glenn of MRC for valuable discussions.

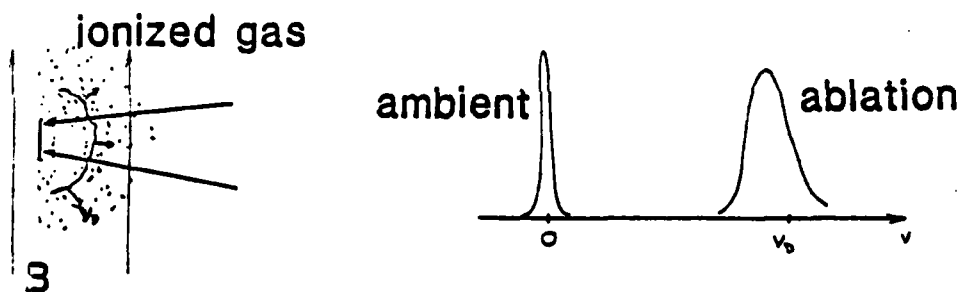
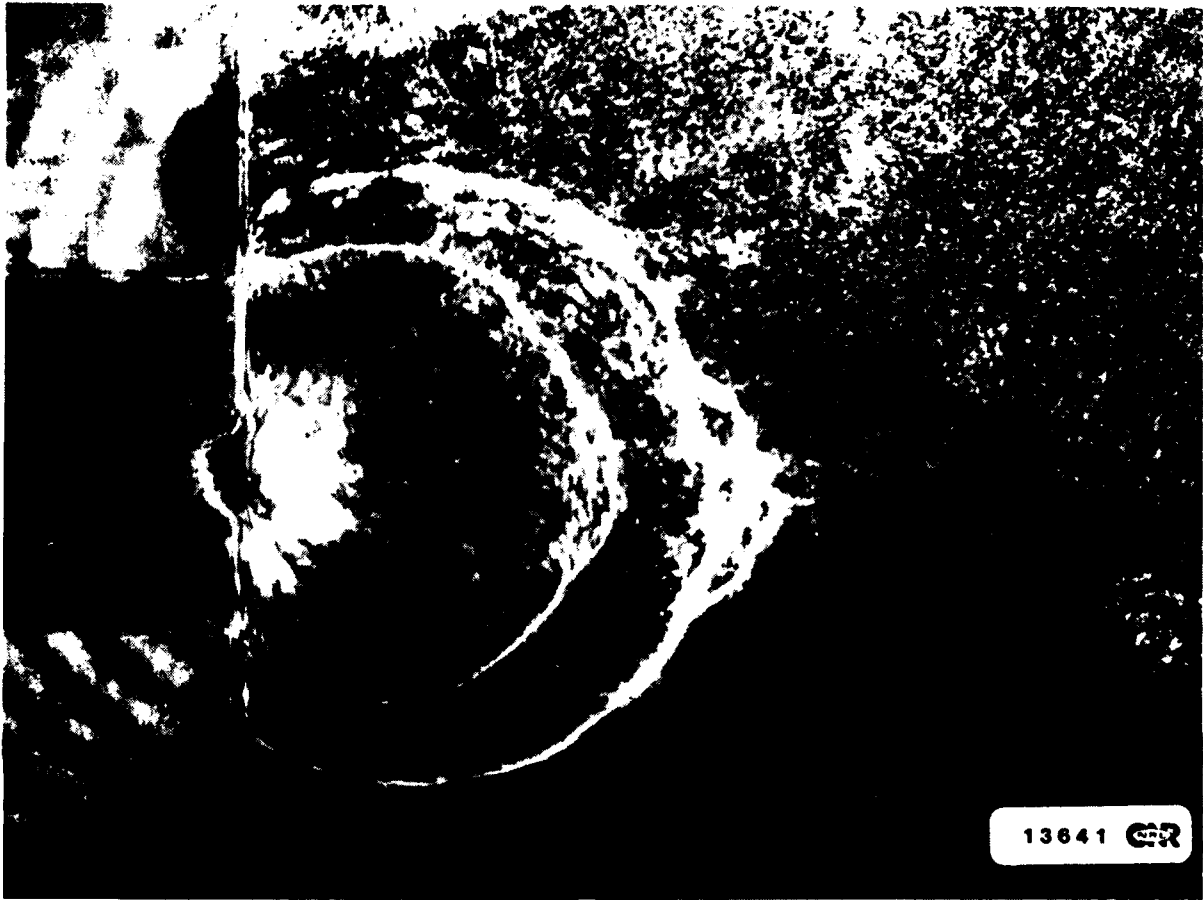


Figure 1 Laser-plasma experiment for debris/ambient plasma coupling (left) and a schematic representation of the debris (ablation) and ambient ion distributions (right).



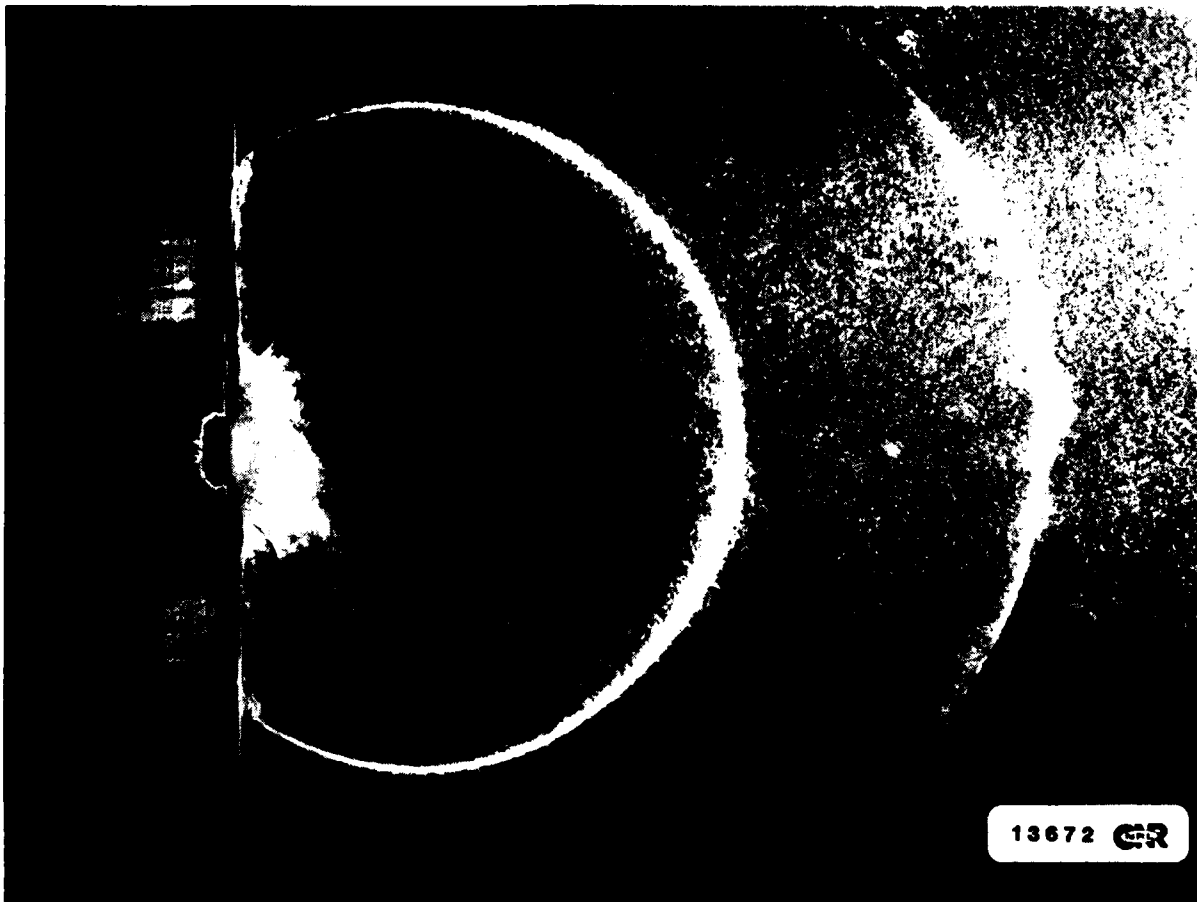
R-1033

Figure 2 Dual-time dark-field shadowgram of shock fronts in a 1.5 Torr (90% N₂ + 10% H₂) gas. The observation times were at 52 and 164 nsec, the incident laser energy was 20 J, the initial debris speed was approximately 3×10^7 cm/sec, and a 630 gauss magnetic field was present into the plane of the paper. The gap in the target holder was about 5 mm.



R-1035

Figure 3 Shadowgram of a shock wave at 52 and 96 nsec in a 5 Torr ambient (N_2+H_2) gas. The laser energy was 38 J and the initial debris speed was 5×10^7 cm/sec. $B=0$. Note the growing "aneurism" at the 4:00 pm position. The object on the right is a magnetic probe (out of focus).



R-1034

Figure 4 Shadowgram of shock waves at 52 and 96 nsec in 5 Torr N_2+H_2 gas. The incident laser energy was 4.1 J and the initial debris velocity was 2×10^7 cm/sec and $B=0$. Note the multiple growing aneurisms.

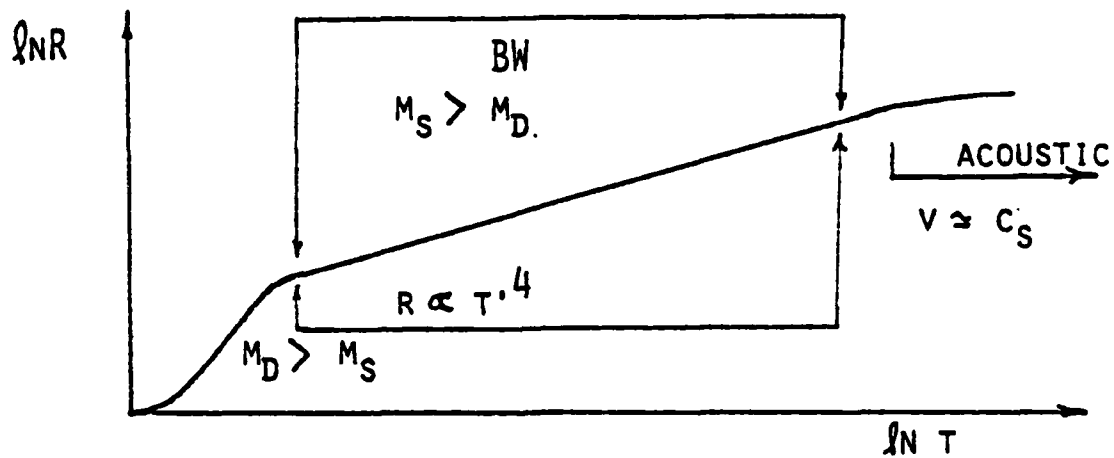


Figure 5 Schematic radius versus time dependence of expansion front. The standard blast-wave regime occurs after the front has picked up several debris masses of ambient material but before the shell speed nears the acoustic speed.

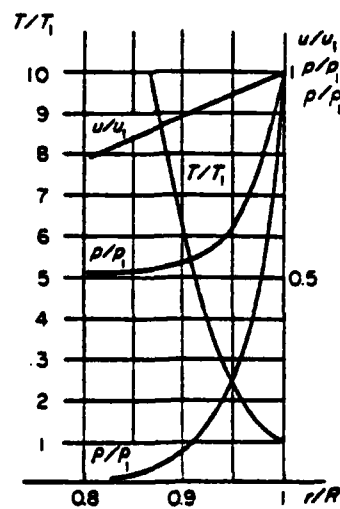


Figure 6 Normalized density ρ , pressure P and flow velocity near the shock front for $\gamma = 1.2$ ideal blast-wave. Note the very thin shell. Taken from Ref. (12).

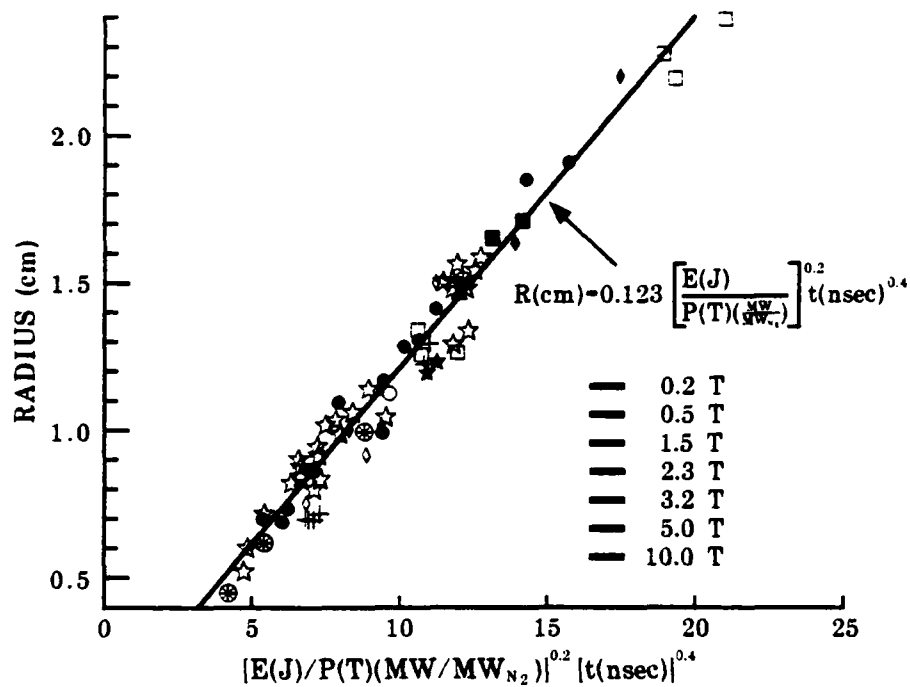


Figure 7 Plot of shock front positions R as a function of the normalized blast-wave scaling parameter for the entire data set outlined in Table I. Note the excellent consistency with blast-wave scaling with $0.092 \zeta_0 = 0.123$.

LOCALIZED THINNING:

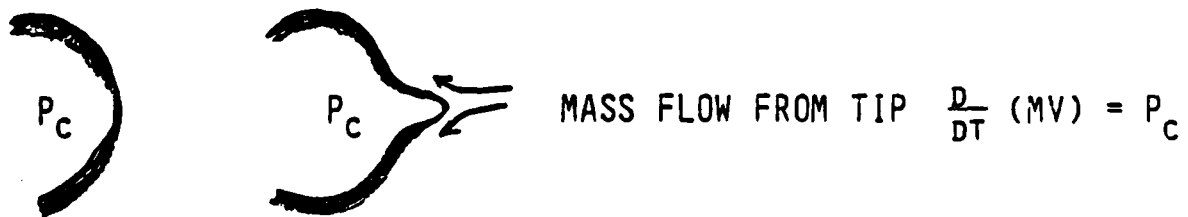


Figure 8 A possible mechanism to cause aneurism-like structure due to the enhanced acceleration of a localized thin region in the coupling front.

References

1. G. Taylor, Proc. Roy. Soc. A201, 159 (1950) and A201, 175 (1950).
2. J. von Neumann and R.D. Richtmyer, J. Appl. Phys. 21, 232 (1950); and H.H. Goldstine and J. von Neumann, Comm. Pure Appl. Math, VIII 327 (1955).
3. L.I. Sedov, "Similarity and Dimensional Methods in Mechanics," (Academic Press, NY, 1959, ed. M. Holt).
4. I.B. Bernstein and D.L. Book, Astrophys. J. 240 223 (1980).
5. R.R. Peterson and G.A. Moses, Nucl. Tech./Fusion 4, 860 (1983).
6. B.H. Ripin, J. Grun, S. Kacenjar, E.A. McLean, and J.A. Stamper, NRL Memo Report #5268 (1984).
7. J.A. Stamper, B.H. Ripin, E.A. McLean, and S.P. Obenschain, NRL Memo Report #5278 (1984).
8. E.A. McLean, J.A. Stamper, H.R. Griem, A.W. Ali, B.H. Ripin, and C.K. Manka, NRL Memo Report #5274 (1984).
9. D.A. Freiwald and R.A. Axford, J. Appl. Phys. 46, 1171 (1975); and D.A. Freiwald, J. Appl. Phys. 43, 2224 (1972).

10. H.L. Brode, J. Appl. Phys. 26, 766 (1955).
11. A.L. Kuhl, M.A. Fry, M. Picone, D.L. Book, and J.P. Boris, NRL Memorandum Report 4613 (1981), "FCT Simulation of HOB Airblast Phenomena," (AD-A107-920).
12. Y.B. Zel'dovich and Y.P. Raizer, "Physics of Shock Waves and High Temperature Hydrodynamic Phenomena, Vol. 1," (Academic Press, NY, 1966).
13. E.G. Harris, NRL Report 4858, "Exact and Approximate Treatments of the One-Dimensional Blast Wave" November 23, 1956 (AD-117 535).
14. B.H. Ripin, R.R. Whitlock, F.C. Young, S.P. Obenschain, E.A. McLean, and R. Decoste, Phys. Rev. Lett. 43, 350 (1979); also see B.H. Ripin et al., Phys. Fluids 23, 1012 (1980) and 24, 990 (1981).
15. J. Grun, S.P. Obenschain, B.H. Ripin, R.R. Whitlock, E.A. McLean, J. Gardner, M.J. Herbst, and J.A. Stamper, Phys. Fluids 26 588 (1983).
16. B.H. Ripin, J. Grun, M.J. Herbst, S.T. Kacenjar, C.K. Manka, E.A. McLean, S.P. Obenschain, and J.A. Stamper, Bull. Am. Phys. Soc. 27, 1041 (1982).
17. D.H. Holland, et al., "Physics of High Altitude Nuclear Burst Effects," MRC Report DNA4501F, pg. 222 (1977). AD-A068-541
18. C. Prettie, (to be published).
19. D. Book, (private communication).

20. C. Longmire, (private communication).
21. M. Keskinen, (private communication).
22. J.A. Stamper, K. Papadopoulos, R.N. Sudan, S.O. Dean, E.A. McLean, and J.M. Dawson, Phys. Rev. Lett. 26, 1012 (1971); and J.A. Stamper and B.H. Ripin, Phys. Rev. Lett. 34, 138 (1975).
23. J.A. Stamper, S.O. Dean, and E.A. McLean in "Laser Interaction and Related Plasma Phenomena," ed. H. Schwarz and H. Hora (Plenum Press, NY, 1972), Vol. 2, pg. 273.
24. G.V. Sklitzkov, in "Laser Interaction and Related Plasma Phenomena," ed. H. Schwarz and H. Hora (Plenum Press, NY, 1971), (Vol. 1), pg. 235; N.G. Basov et al., in "Laser Interaction and Related Plasma Phenomena," ed. H. Schwarz and H. Hora (Plenum Press, NY, 1974), Vol. 3B, pg. 553; D.M. Wilke, Los Alamos Report LA-9182-T (1982).
25. R. Kilb, (private communication); see also A.W. Gregersen, F.E. Fajen, R.W. Kilb and W.W. White, (private communication).

DISTRIBUTION LIST

DEPARTMENT OF DEFENSE

ASSISTANT SECRETARY OF DEFENSE
COMM, CMD, CONT 7 INTELL
WASHINGTON, D.C. 20301

DIRECTOR
COMMAND CONTROL TECHNICAL CENTER
PENTAGON RM BE 685
WASHINGTON, D.C. 20301
O1CY ATTN C-650
O1CY ATTN C-312 R. MASON

DIRECTOR
DEFENSE ADVANCED RSCH PROJ AGENCY
ARCHITECT BUILDING
1400 WILSON BLVD.
ARLINGTON, VA. 22209
O1CY ATTN NUCLEAR MONITORING RESEARCH
O1CY ATTN STRATEGIC TECH OFFICE

DEFENSE COMMUNICATION ENGINEER CENTER
1860 WIEHLE AVENUE
RESTON, VA. 22090
O1CY ATTN CODE R410
O1CY ATTN CODE R812

DEFENSE TECHNICAL INFORMATION CENTER
CAMERON STATION
ALEXANDRIA, VA. 22314
O2CY

DIRECTOR
DEFENSE NUCLEAR AGENCY
WASHINGTON, D.C. 20305
O1CY ATTN STVL
O4CY ATTN TITL
O1CY ATTN DDST
O3CY ATTN RAAZ

COMMANDER
FIELD COMMAND
DEFENSE NUCLEAR AGENCY
KIRTLAND, AFB, NM 87115
O1CY ATTN FCPR

DIRECTOR
INTERSERVICE NUCLEAR WEAPONS SCHOOL
KIRTLAND AFB, NM 87115
O1CY ATTN DOCUMENT CONTROL

JOINT CHIEFS OF STAFF
WASHINGTON, D.C. 20301
O1CY ATTN J-3 WWMCCS EVALUATION OFFICE

DIRECTOR
JOINT STRAT TGT PLANNING STAFF
OFFUTT AFB
OMAHA, NE 68113
O1CY ATTN JLTW-2
O1CY ATTN JPST G. GOETZ

CHIEF
LIVERMORE DIVISION FLD COMMAND DNA
DEPARTMENT OF DEFENSE
LAWRENCE LIVERMORE LABORATORY
P.O. BOX 808
LIVERMORE, CA 94550
O1CY ATTN FCPRL

COMMANDANT
NATO SCHOOL (SHAPE)
APO NEW YORK 09172
O1CY ATTN U.S. DOCUMENTS OFFICER

UNDER SECY OF DEF FOR RSCH & ENGRG
DEPARTMENT OF DEFENSE
WASHINGTON, D.C. 20301
O1CY ATTN STRATEGIC & SPACE SYSTEMS (OS)

WWMCCS SYSTEM ENGINEERING ORG
WASHINGTON, D.C. 20305
O1CY ATTN R. CRAWFORD

COMMANDER/DIRECTOR
ATMOSPHERIC SCIENCES LABORATORY
U.S. ARMY ELECTRONICS COMMAND
WHITE SANDS MISSILE RANGE, NM 88002
O1CY ATTN DELAS-EO F. NILES

DIRECTOR
BMD ADVANCED TECH CTR
HUNTSVILLE OFFICE
P.O. BOX 1500
HUNTSVILLE, AL 35807
O1CY ATTN ATC-T MELVIN T. CAPPS
O1CY ATTN ATC-O W. DAVIES
O1CY ATTN ATC-R DON RUSS

PROGRAM MANAGER
BMD PROGRAM OFFICE
5001 EISENHOWER AVENUE
ALEXANDRIA, VA 22333
O1CY ATTN DACS-BMT J. SHEA

CHIEF C-E- SERVICES DIVISION
U.S. ARMY COMMUNICATIONS CMD
PENTAGON RM 1B269
WASHINGTON, D.C. 20310
O1CY ATTN C- E-SERVICES DIVISION

COMMANDER
FRADCOM TECHNICAL SUPPORT ACTIVITY
DEPARTMENT OF THE ARMY
FORT MONMOUTH, N.J. 07703
O1CY ATTN DRSEL-NL-RD H. BENNET
O1CY ATTN DRSEL-PL-ENV H. BOMKE
O1CY ATTN J.E. QUIGLEY

COMMANDER
U.S. ARMY COMM-ELEC ENGRG INSTAL AGY
FT. HUACHUCA, AZ 85613
O1CY ATTN CCC-EMEO GEORGE LANE

COMMANDER
U.S. ARMY FOREIGN SCIENCE & TECH CTR
220 7TH STREET, NE
CHARLOTTESVILLE, VA 22901
O1CY ATTN DRXST-SD

COMMANDER
U.S. ARMY MATERIAL DEV & READINESS CMD
5001 EISENHOWER AVENUE
ALEXANDRIA, VA 22333
O1CY ATTN DRCLDC J.A. BENDER

COMMANDER
U.S. ARMY NUCLEAR AND CHEMICAL AGENCY
7500 BACKLICK ROAD
BLDG 2073
SPRINGFIELD, VA 22150
O1CY ATTN LIBRARY

DIRECTOR
U.S. ARMY BALLISTIC RESEARCH LABORATORY
ABERDEEN PROVING GROUND, MD 21005
O1CY ATTN TECH LIBRARY EDWARD BAICY

COMMANDER
U.S. ARMY SATCOM AGENCY
FT. MONMOUTH, NJ 07703
O1CY ATTN DOCUMENT CONTROL

COMMANDER
U.S. ARMY MISSILE INTELLIGENCE AGENCY
REDSTONE ARSENAL, AL 35809
O1CY ATTN JIM GAMBLE

DIRECTOR
U.S. ARMY TRADOC SYSTEMS ANALYSIS ACTIVITY
WHITE SANDS MISSILE RANGE, NM 88002
O1CY ATTN ATAA-SA
O1CY ATTN TCC/F. PAYAN JR.
O1CY ATTN ATIA-TAC LTC J. HESSE

COMMANDER
NAVAL ELECTRONIC SYSTEMS COMMAND
WASHINGTON, D.C. 20360
O1CY ATTN NAVALEX 034 T. HUGHES
O1CY ATTN PME 117
O1CY ATTN PME 117-T
O1CY ATTN CODE 5011

COMMANDING OFFICER
NAVAL INTELLIGENCE SUPPORT CTR
4301 SUITLAND ROAD, BLDG. 5
WASHINGTON, D.C. 20390
O1CY ATTN MR. DUBBIN STIC 12
O1CY ATTN NISC-50
O1CY ATTN CODE 5404 J. GALET

COMMANDER
NAVAL OCEAN SYSTEMS CENTER
SAN DIEGO, CA 92152
O1CY ATTN J. FERGUSON

NAVAL RESEARCH LABORATORY
WASHINGTON, DC 20375

01CY ATTN CODE 4700 S.L. OSSAKOW
26 CYS IF UNCLASS, 1 CY IF CLASS
01CY ATTN CODE 4701 I. VITKOVITSKY
01CY ATTN CODE 4780 J. Huba (10
CYS IF UNCLASS, 1 CY IF CLASS)
01CY ATTN CODE 7500
01CY ATTN CODE 7550
01CY ATTN CODE 7580
01CY ATTN CODE 7551
01CY ATTN CODE 7555
01CY ATTN CODE 4730 E. MCLEAN
01CY ATTN CODE 4108
01CY ATTN CODE 4730 B. RIPIN
22CY ATTN CODE 2628
100CY ATTN CODE 4730

COMMANDER
NAVAL SEA SYSTEMS COMMAND
WASHINGTON, DC 20362
01CY ATTN CAPT R. PITKIN

COMMANDER
NAVAL SPACE SURVEILLANCE SYSTEM
DAHLGREN, VA 22448
01CY ATTN CAPT J.H. BURTON

OFFICER-IN-CHARGE
NAVAL SURFACE WEAPONS CENTER
WHITE OAK, SILVER SPRING, MD 20910
01CY ATTN CODE F31

DIRECTOR
STRATEGIC SYSTEMS PROJECT OFFICE
DEPARTMENT OF THE NAVY
WASHINGTON, DC 20376
01CY ATTN NSP-2141
01CY ATTN Nssp-2722 FRED WIMBERLY

COMMANDER
NAVAL SURFACE WEAPONS CENTER
DAHLGREN LABORATORY
DAHLGREN, VA 22448
01CY ATTN CODE DF-14 R. BUTLER

OFFICE OF NAVAL RESEARCH
ARLINGTON, VA 222L7
01CY ATTN CODE 465
01CY ATTN CODE 461
01CY ATTN CODE 402
01CY ATTN CODE 420
01CY ATTN CODE 421

COMMANDER
AEROSPACE DEFENSE COMMAND/DC
DEPARTMENT OF THE AIR FORCE
ENT AFB, CO 90812
01CY ATTN DC MR. LONG

COMMANDER AEROSPACE DEFENSE COMMAND/XPD
DEPARTMENT OF THE AIR FORCE
ENT AFB, CO 80912
01CY ATTN XPDQQ
01CY ATTN XP

AIR FORCE GEOPHYSICS LABORATORY
HANSCOM AFB, MA 01731
01CY ATTN OPR HAROLD GARDNER
01CY ATTN LKB KENNETH S.W. CHAMPION
01CY ATTN OPR ALVA T. STAIR
01CY ATTN PHD JURGEN BUCHAU
01CY ATTN PHD JOHN P. MULLEN

AF WEAPONS LABORATORY
KIRTLAND AFB, NM 87117
01CY ATTN SUL
01CY ATTN CA ARTHUR H. GUENTHER
01CY ATTN NTYCE LT. G. KRAJEI

AFTAC
PATRICK AFB, FL 32925
01CY ATTN TF/MAJ WILEY
01CY ATTN TN

AIR FORCE AVIONICS LABORATORY
WRIGHT-PATTERSON AFB, OH 45433
01CY ATTN AAD WADE HUNT
01CY ATTN AAD ALLEN JOHNSON

DEPUTY CHIEF OF STAFF
RESEARCH, DEVELOPMENT, & ACQ
DEPARTMENT OF THE AIR FORCE
WASHINGTON, DC 20030
01CY ATTN AFRDQ

HEADQUARTERS
ELECTRONIC SYSTEMS DIVISION
DEPARTMENT OF THE AIR FORCE
HANSCOM AFB, MA 01731
01CY ATTN J. DEAS

HEADQUARTERS
ELECTRONIC SYSTEMS DIVISION/YSEA
DEPARTMENT OF THE AIR FORCE
HANSCOM AFB, MA 01732
01CY ATTN YSEA

HEADQUARTERS
ELECTRONIC SYSTEMS DIVISION/DC
DEPARTMENT OF THE AIR FORCE
HANSCOM AFB, MA 01731
O1CY ATTN DCKC MAJ J.C. CLARK

COMMANDER
FOREIGN TECHNOLOGY DIVISION, AFSC
WRIGHT-PATTERSON AFB, OH 45433
O1CY ATTN NICD LIBRARY
O1CY ATTN ETRP B. BALLARD

COMMANDER
ROME AIR DEVELOPMENT CENTER, AFSC
GRIFFISS AFB, NY 13441
O1CY ATTN DOC LIBRARY/TSLD
O1CY ATTN OCSE V. COYNE

SAMSO/SZ
POST OFFICE BOX 92960
WORLDWAY POSTAL CENTER
LOS ANGELES, CA 90009
(SPACE DEFENSE SYSTEMS)
O1CY ATTN SZJ

STRATEGIC AIR COMMAND/XPFS
OFFUTT AFB, NE 68113
O1CY ATTN ADWATE MAJ BRUCE BAUER
O1CY ATTN NRT
O1CY ATTN DOK CHIEF SCIENTIST

SAMSO/SK
P.O. BOX 92960
WORLDWAY POSTAL CENTER
LOS ANGELES, CA 90009
O1CY ATTN SKA (SPACE COMM SYSTEMS)
M. CLAVIN

SAMSO/MN
NORTON AFB, CA 92409
(MINUTEMAN)
O1CY ATTN MNWL

COMMANDER
ROME AIR DEVELOPMENT CENTER, AFSC
HANSCOM AFB, MA 01731
O1CY ATTN EEP A. LORENTZEN

DEPARTMENT OF ENERGY
LIBRARY ROOM G-042
WASHINGTON, D.C. 20545
O1CY ATTN DOC CON FOR A. LABOWITZ

DEPARTMENT OF ENERGY
ALBUQUERQUE OPERATIONS OFFICE
P.O. BOX 5400
ALBUQUERQUE, NM 87115
O1CY ATTN DOC CON FOR D. SHERWOOD

EG&G, INC.
LOS ALAMOS DIVISION
P.O. BOX 809
LOS ALAMOS, NM 85544
O1CY ATTN DOC CON FOR J. BREEDLOVE

UNIVERSITY OF CALIFORNIA
LAWRENCE LIVERMORE LABORATORY
P.O. BOX 808
LIVERMORE, CA 94550
O1CY ATTN DOC CON FOR TECH INFO DEPT
O1CY ATTN DOC CON FOR L-389 R. OTT
O1CY ATTN DOC CON FOR L-31 R. HAGER
O1CY ATTN DOC CON FOR L-46 P. SEWARD

LOS ALAMOS NATIONAL LABORATORY
P.O. BOX 1663
LOS ALAMOS, NM 87545
O1CY ATTN DOC CON FOR J. WOLCOTT
O1CY ATTN DOC CON FOR R.F. TASCHEK
O1CY ATTN DOC CON FOR E. JONES
O1CY ATTN DOC CON FOR J. MALIK
O1CY ATTN DOC CON FOR R. JEFFRIES
O1CY ATTN DOC CON FOR J. ZINN
O1CY ATTN DOC CON FOR P. KEATON
O1CY ATTN DOC CON FOR D. WESTERVELT
O1CY ATTN D. SAPPENFIELD

SANDIA LABORATORIES
P.O. BOX 5800
ALBUQUERQUE, NM 87115
O1CY ATTN DOC CON FOR W. BROWN
O1CY ATTN DOC CON FOR A. THORNBROUGH
O1CY ATTN DOC CON FOR T. WRIGHT
O1CY ATTN DOC CON FOR D. DAHLGREN
O1CY ATTN DOC CON FOR 3141
O1CY ATTN DOC CON FOR SPACE PROJECT DIV

SANDIA LABORATORIES
LIVERMORE LABORATORY
P.O. BOX 969
LIVERMORE, CA 94550
O1CY ATTN DOC CON FOR B. MURPHEY
O1CY ATTN DOC CON FOR T. COOK

OFFICE OF MILITARY APPLICATION
DEPARTMENT OF ENERGY
WASHINGTON, D.C. 20545
O1CY ATTN DOC CON DR. YO SONG

OTHER GOVERNMENT

DEPARTMENT OF COMMERCE
NATIONAL BUREAU OF STANDARDS
WASHINGTON, D.C. 20234
01CY (ALL CORRES: ATTN SEC OFFICER FOR)

INSTITUTE FOR TELECOM SCIENCES
NATIONAL TELECOMMUNICATIONS & INFO ADMIN
BOULDER, CO 80303
01CY ATTN A. JEAN (UNCLASS ONLY)
01CY ATTN W. UTLAUT
01CY ATTN D. CROMBIE
01CY ATTN L. BERRY

NATIONAL OCEANIC & ATMOSPHERIC ADMIN
ENVIRONMENTAL RESEARCH LABORATORIES
DEPARTMENT OF COMMERCE
BOULDER, CO 80302
01CY ATTN R. GRUBB
01CY ATTN AERONOMY LAB G. REID

DEPARTMENT OF DEFENSE CONTRACTORS

AEROSPACE CORPORATION
P.O. BOX 92957
LOS ANGELES, CA 90009
01CY ATTN I. GARFUNKEL
01CY ATTN T. SALMI
01CY ATTN V. JOSEPHSON
01CY ATTN S. BOWER
01CY ATTN D. OLSEN

ANALYTICAL SYSTEMS ENGINEERING CORP
5 OLD CONCORD ROAD
BURLINGTON, MA 01803
01CY ATTN RADIO SCIENCES

AUSTIN RESEARCH ASSOC., INC.
1901 RUTLAND DRIVE
AUSTIN, TX 78758
01CY ATTN L. SLOAN
01CY ATTN R. THOMPSON

BERKELEY RESEARCH ASSOCIATES, INC.
P.O. BOX 983
BERKELEY, CA 94701
01CY ATTN J. WORKMAN
01CY ATTN C. PRETTIE
01CY ATTN S. BRECHT

BOEING COMPANY, THE
P.O. BOX 3707
SEATTLE, WA 98124
01CY ATTN G. KEISTER
01CY ATTN D. MURRAY
01CY ATTN G. HALL
01CY ATTN J. KENNEY

CHARLES STARK DRAPER LABORATORY, INC.
555 TECHNOLOGY SQUARE
CAMBRIDGE, MA 02139
01CY ATTN D.B. COX
01CY ATTN J.P. GILMORE

COMSAT LABORATORIES
LINTHICUM ROAD
CLARKSBURG, MD 20734
01CY ATTN G. HYDE

CORNELL UNIVERSITY
DEPARTMENT OF ELECTRICAL ENGINEERING
ITHACA, NY 14850
01CY ATTN D.T. FARLEY, JR.

ELECTROSPACE SYSTEMS, INC.
BOX 1359
RICHARDSON, TX 75080
01CY ATTN H. LOGSTON
01CY ATTN SECURITY (PAUL PHILLIPS)

EOS TECHNOLOGIES, INC.
606 Wilshire Blvd.
Santa Monica, Calif 90401
01CY ATTN C.B. GABBARD

ESL, INC.
495 JAVA DRIVE
SUNNYVALE, CA 94086
01CY ATTN J. ROBERTS
01CY ATTN JAMES MARSHALL

GENERAL ELECTRIC COMPANY
SPACE DIVISION
VALLEY FORGE SPACE CENTER
GODDARD BLVD KING OF PRUSSIA
P.O. BOX 8555
PHILADELPHIA, PA 19101
01CY ATTN M.H. BORTNER SPACE SCI LAB

GENERAL ELECTRIC COMPANY
P.O. BOX 1122
SYRACUSE, NY 13201
01CY ATTN F. REIBERT

GENERAL ELECTRIC TECH SERVICES CO., INC.
INES
COURT STREET
SYRACUSE, NY 13201
O1CY ATTN G. MILLMAN

GEOPHYSICAL INSTITUTE
UNIVERSITY OF ALASKA
FAIRBANKS, AK 99701
(ALL CLASS ATTN: SECURITY OFFICER)
O1CY ATTN T.N. DAVIS (UNCLASS ONLY)
O1CY ATTN TECHNICAL LIBRARY
O1CY ATTN NEAL BROWN (UNCLASS ONLY)

GTE SYLVANIA, INC.
ELECTRONICS SYSTEMS GRP-EASTERN DIV
77 A STREET
NEEDHAM, MA 02194
O1CY ATTN DICK STEINHOF

HSS, INC.
2 ALFRED CIRCLE
BEDFORD, MA 01730
O1CY ATTN DONALD HANSEN

ILLINOIS, UNIVERSITY OF
107 COBLE HALL
150 DAVENPORT HOUSE
CHAMPAIGN, IL 61820
(ALL CORRES ATTN DAN MCCLELLAND)
O1CY ATTN K. YEH

INSTITUTE FOR DEFENSE ANALYSES
1801 NO. BEAUREGARD STREET
ALEXANDRIA, VA 22311
O1CY ATTN J.M. AFIN
O1CY ATTN ERNEST BAUER
O1CY ATTN HANS WOLFARD
O1CY ATTN JOEL BENGSTON

INTL TEL & TELEGRAPH CORPORATION
500 WASHINGTON AVENUE
NUTLEY, NJ 07110
O1CY ATTN TECHNICAL LIBRARY

JAYCOR
11011 TORREYANA ROAD
P.O. BOX 85154
SAN DIEGO, CA 92138
O1CY ATTN J.L. SPERLING

JOHNS HOPKINS UNIVERSITY
APPLIED PHYSICS LABORATORY
JOHNS HOPKINS ROAD
LAUREL, MD 20810
O1CY ATTN DOCUMENT LIBRARIAN
O1CY ATTN THOMAS POTEMBA
O1CY ATTN JOHN DASSOULAS

KAMAN SCIENCES CORP
P.O. BOX 7463
COLORADO SPRINGS, CO 80933
O1CY ATTN T. MEAGHER

KAMAN TEMPO-CENTER FOR ADVANCED STUDIES
816 STATE STREET (P.O DRAWER QQ)
SANTA BARBARA, CA 93102
O1CY ATTN DASIAC
O1CY ATTN WARREN S. KNAPP
O1CY ATTN WILLIAM MCNAMARA
O1CY ATTN B. GAMBILL

LINKABIT CORP
10453 ROSELLE
SAN DIEGO, CA 92121
O1CY ATTN IRWIN JACOBS

LOCKHEED MISSILES & SPACE CO., INC
P.O. BOX 504
SUNNYVALE, CA 94088
O1CY ATTN DEPT 60-12
O1CY ATTN D.R. CHURCHILL

LOCKHEED MISSILES & SPACE CO., INC.
3251 HANOVER STREET
PALO ALTO, CA 94304
O1CY ATTN MARTIN WALT DEPT 52-12
O1CY ATTN W.L. IMHOF DEPT 52-12
O1CY ATTN RICHARD G. JOHNSON DEPT 52-12
O1CY ATTN J.B. CLADIS DEPT 52-12

MARTIN MARIETTA CORP
ORLANDO DIVISION
P.O. BOX 5837
ORLANDO, FL 32805
O1CY ATTN R. HEFFNER

MCDONNELL DOUGLAS CORPORATION
5301 BOLSA AVENUE
HUNTINGTON BEACH, CA 92647
01CY ATTN N. HARRIS
01CY ATTN J. MOULE
01CY ATTN GEORGE MROZ
01CY ATTN W. OLSON
01CY ATTN R.W. HALPRIN
01CY ATTN TECHNICAL LIBRARY SERVICES

MISSION RESEARCH CORPORATION
735 STATE STREET
SANTA BARBARA, CA 93101
01CY ATTN P. FISCHER
01CY ATTN W.F. CREVIER
01CY ATTN STEVEN L. GUTSCHE
01CY ATTN R. BOGUSCH
01CY ATTN R. HENDRICK
01CY ATTN RALPH KILB
01CY ATTN DAVE SOWLE
01CY ATTN F. FAJEN
01CY ATTN M. SCHEIBE
01CY ATTN CONRAD L. LONGMIRE
01CY ATTN B. WHITE

MISSION RESEARCH CORPORATION
1720 RANDOLPH ROAD, SE
ALBUQUERQUE, NM 87106
01CY ATTN R. STELLINGWERF
01CY ATTN M. ALME
01CY ATTN L. WRIGHT

MITRE CORPORATION, THE
P.O. BOX 208
BEDFORD, MA 01730
01CY ATTN JOHN MORGANSTERN
01CY ATTN G. HARDING
01CY ATTN C.E. CALLARAN

MITRE CORPORATION
WESTGATE RESEARCH PARK
1820 DOLLY MADISON BLVD.
MCLEAN, VA 22101
01CY ATTN W. HALL
01CY ATTN W. FOSTER

PACIFIC-SIERRA RESEARCH CORP.
12340 SANTA MONICA BLVD.
LOS ANGELES, CA 90025
01CY ATTN E.C. FIELD, JR.

PENNSYLVANIA STATE UNIVERSITY
IONOSPHERE RESEARCH LAB
318 ELECTRICAL ENGINEERING EAST
UNIVERSITY PARK, PA 16802
(NO CLASS. TO THIS ADDRESS)
01CY ATTN IONOSPHERIC RESEARCH LAB

PHOTOMETRICS, INC.
4 ARROW DRIVE
WOBBURN, MA 01801
01CY ATTN IRVING L. KOFSKY

PHYSICAL DYNAMICS, INC.
P.O. BOX 3027
BELLEVUE, WA 98009
01CY ATTN E.J. FREMOUW

PHYSICAL DYNAMICS, INC.
P.O. BOX 10367
OAKLAND, CA 94610
01CY ATTN A. THOMSON

R&D ASSOCIATES
P.O. BOX 9695
MARINA DEL REY, CA 90291
01CY ATTN FORREST GILMORE
01CY ATTN WILLIAM B. WRIGHT, JR.
01CY ATTN ROBERT F. LELEVIER
01CY ATTN WILLIAM J. KARZAS
01CY ATTN R. ORY
01CY ATTN C. MACDONALD
01CY ATTN R. TURCO
01CY ATTN L. DeRADD

RAND CORPORATION, THE
1700 MAIN STREET
SANTA MONICA, CA 90406
01CY ATTN CULLEN CRAIN
01CY ATTN ED BEDROZIAN

RAYTHEON COMPANY
528 BOSTON POST ROAD
SUDBURY, MA 01776
01CY ATTN BARBARA ADAMS

SCIENCE APPLICATIONS, INC.
P.O. BOX 2351
LA JOLLA, CA 92038

01CY ATTN LEWIS M. LINSON
01CY ATTN DANIEL A. HAMLIN
01CY ATTN E. FRIEMAN
01CY ATTN E.A. STRAKER
01CY ATTN CURTIS A. SMITH
01CY ATTN JACK MCDUGALL

SCIENCE APPLICATIONS, INC
1710 GOODRIDGE DR.
MCLEAN, VA 22102
ATTN: J. COCKAYNE

SRI INTERNATIONAL
333 RAVENSWOOD AVENUE
MENLO PARK, CA 94025

01CY ATTN DONALD NEILSON
01CY ATTN ALAN BURNS
01CY ATTN G. SMITH
01CY ATTN R. TSUNODA
01CY ATTN DAVID A. JOHNSON
01CY ATTN WALTER G. CHESNUT
01CY ATTN CHARLES L. RINO
01CY ATTN WALTER JAYE
01CY ATTN J. VICKREY
01CY ATTN RAY L. LEADABRAND
01CY ATTN G. CARPENTER
01CY ATTN G. PRICE
01CY ATTN R. LIVINGSTON
01CY ATTN V. GONZALES
01CY ATTN D. MCDANIEL

TECHNOLOGY INTERNATIONAL CORP
75 WIGGINS AVENUE
BEDFORD, MA 01730
01CY ATTN W.P. BOQUIST

TOYON RESEARCH CO.
P.O. Box 6890
SANTA BARBARA, CA 93111
01CY ATTN JOHN ISE, JR.
01CY ATTN JOEL GABBARINO

TRW DEFENSE & SPACE SYS GROUP
ONE SPACE PARK

REDONDO BEACH, CA 90278
01CY ATTN R. K. PLEBUCH
01CY ATTN S. ALTSCHULER
01CY ATTN D. DEE
01CY ATTN D/ STOCKWELL
SNTF/1575

VISIDYNE
SOUTH BEDFORD STREET
BURLINGTON, MASS 01803
01CY ATTN W. REIDY
01CY ATTN J. CARPENTER
01CY ATTN C. HUMPHREY

END

FILMED

5-84

DTIC